Published in final edited form as:
Biomaterials. 2013 July ; 34(21): 5328–5335. doi:10.1016/j.biomaterials.2013.03.059.

The Architecture and Biological Performance of Drug-Loaded LbL Nanoparticles

Stephen Morton[1,2], **Zhiyong Poon**[2], and **Paula Hammond**[1,2,*]

[1]Department of Chemical Engineering, Massachusetts Institute of Technology

[2]Koch Institute for Integrative Cancer Research, Massachusetts Institute of Technology

Abstract

Layer-by-Layer (LbL) nanoparticles are an emerging class of therapeutic carriers that afford precise control over key design parameters that facilitate improved drug and carrier pharmacokinetics, and enhanced molecular-targeting capabilities. This paper advances the development of these systems by establishing them as drug carriers, with the means to control drug release in a systemic environment and retard particle clearance from circulation, promoting improved biodistribution of the drug-containing system. Using dual-fluorescent tracking *in vivo*, this work establishes a robust means of screening libraries of LbL systems generated, affording simultaneous resolution over persistence and biodistribution of both the drug and carrier following systemic administration of a single particle formulation. Employing a PLGA drug-containing core as a substrate for LbL deposition, a range of coated systems were fabricated to investigate the abilities of these films to stabilize drug for delivery as well as to improve the pharmacokinetics of both the drug and carrier. Significant reductions in liver accumulation were observed for different formulations of the layered architectures within the first 30 minutes of systemic circulation. LbL architectures diminished liver localization of the surrogate drug, cardiogreen, by 10–25% ID/g relative to native PLGA nanoparticles and modulated carrier accumulation in the liver >50% ID/g. Further, enhanced persistence of the drug was observed with the coated systems, significantly increasing the drug half-life from 2–3 minutes for free drug and 1.87h for the uncoated core to 4.17h and 4.54h for the coated systems. These systems provide an exciting, modular platform that improves the pharmacokinetic properties of the therapeutic, reduces bolus release of drug from nanoparticles, and enhances the safety and circulation half-life of the drug *in vivo*, proving them to be highly clinically-relevant and a promising approach for future development of molecularly-targeted and combination therapeutics.

Keywords

Nanoparticle; Fluorescence; Drug delivery; Surface modification

*Corresponding author: Paula Hammond - Massachusetts Institute of Technology, Rm 76-553, Cambridge, MA 02139; (ph) 617-258-7577; (f) 617-253-8557; hammond@mit.edu.
Stephen Morton - Massachusetts Institute of Technology, Rm 76-553, Cambridge, MA 02139; swmorton@mit.edu
Zhiyong Poon - - Massachusetts Institute of Technology, Rm 76-553, Cambridge, MA 02139; pzy1234@gmail.com

Introduction

Layer-by-Layer (LbL) assembly of polyelectrolytes on solid substrates is a well-characterized, tunable approach[1] for generating functional thin films for a variety of applications, including drug and gene delivery[2–5] and tissue engineering.[6, 7] For these applications, this technique is advantageous in that the incorporation of a broad range of therapeutics (e.g., proteins, nucleic acids, and small-molecule drugs) is carried out under physiological conditions, non-covalently, thereby preserving the native properties of the cargo while stabilizing it for delivery. Furthermore, surface-limited, sequential adsorption affords nano-scale precision over the composition of each layer; these advantages, when combined with the ability to incorporate a broad range of therapeutics and materials with diverse functionalities, greatly facilitate the development of drug delivery platforms with sophisticated control over the spatial and temporal release of film constituents.

While LbL has been successfully implemented on macroscopic surfaces with great promise for many biomedical applications[4, 8–15], it has been a challenge to coat nanoscale materials systems and achieve particles that can be sustained for systemic delivery[5]. Work with gold nanoparticles has demonstrated the ability to generate conformal LbL coatings on nanoscale templates, opening new and exciting opportunities for nanoparticle technologies with applications in drug and nucleic acid delivery[16–27]; however, the translation of LbL-based nanocarriers for systemic applications requires further examination of how LbL film architectures can be manipulated to overcome systemic delivery barriers and to sustain drug delivery in such complex biological settings. In our recent work, we investigated the impact of different nanoparticle-bound film architectures on physiological stability, elucidating key control variables necessary to generate a serum-stable particle, as well as the effect of terminal polymer layers on subsequent biodistribution of the nanocarriers.[28] LbL architectures that act as highly effective stabilizing layers were demonstrated to impart long circulation times and EPR-based (Enhanced Permeability and Retention) passive targeting to the resulting systems.[29] We have also developed dynamic LbL layers that ‘shed’ at the lower pH of hypoxic tumor microenvironments and subsequently reveal a positively charged surface that rapidly mediates uptake by tumor cells.[30] Similar demonstrations of dynamic LbL particle design for tumor targeting,[31] along with the ability of LbL nanofilms to modulate biodistribution, lay a framework for continued development of LbL-based nanoparticles towards built-to-order systems that are key for unlocking new biomedical opportunities for these platforms.

As LbL nanoparticle technology moves towards clinical translation, it is essential to establish these systems as drug-stabilizing carriers; the focus of this work is on small molecule therapeutics. The challenges and approaches to small molecule delivery are well documented[32]; characteristic bolus release upon injection is one of the most significant limitations to efficacious treatment for this class of therapeutics.[32] Once it is freed from the carrier, drug is often rapidly cleared, reducing its plasma concentration, and producing significant off-target cytotoxicity. The ability to control small molecule release and drug distribution at a cellular and tissue level is, therefore, an active area of investigation. Further, little information regarding the real-time fate of small molecule release from delivery platforms *in vivo* is understood following systemic administration. The current work seeks to

demonstrate LbL nanoparticle material systems as viable candidates for small molecule drug delivery, as well as to develop a robust, systematic approach for screening a library of materials for incorporation in these engineered systems. LbL films have been previously demonstrated as effective small molecule delivery agents,[33, 34] with an enhanced level of control over release. This work examines LbL architectures as dually functional films on nanoparticle surfaces – acting as membranes that control rate of drug release from the nanoparticle core and thus impact pharmacokinetics of the drug, as well as the hydrated, protein-resistive coatings that modulate blood circulation half-life and biodistribution for both the drug and carrier. The current study probes a series of nanoparticle architectures assembled on a biodegradable poly(lactic-co-glycolic acid) (PLGA) drug-loaded nanoparticle core. Using *in vivo* imaging for simultaneous drug and particle fluorescence tracking *in vivo*, this work provides a framework for assessment of LbL nanoparticles as small molecule delivery agents. This technique for live animal imaging is a convenient and robust means of probing delivery pharmacokinetics and biodistribution. It affords the capability of drug and particle monitoring following administration to a single animal, allowing for high throughput *in vivo* screening of delivery systems. The current study demonstrates this capacity, evaluating LbL nanoparticles using multiple indicators of stability and performance, in an effort to advance the technology towards therapeutic settings.

Materials and Methods

All chemicals were purchased from Sigma-Aldrich, except for hyaluronic acid (Lifecore Biomedical) and doxorubicin-HCl (LC Laboratories). Release dialysis float-a-lyzers were purchased from Spectrum Laboratories. NCR nude and BALB/C female mice were furnished by Taconic.

Nanoparticle Synthesis

PLGA particles were prepared under aseptic conditions via an emulsification-diffusion method with slight modifications to a previously established protocol.[35] Briefly, 50 mg PLGA was dissolved in 3 mL acetone with 0.5 mL of 10mg/mL drug (cardiogreen/ doxorubicin) in methanol. This solution was subsequently added to 10mL 10% BSA in PBS and sonicated at RT. The emulsion was stirred overnight at 1000 rpm. The resulting particle suspension was purified via centrifugation (15,000 g, 30 min) prior to LbL assembly. LbL assembly was conducted by introducing ~10% of the recovered drug-loaded nanoparticles in excess polyelectrolyte solution (5 mg/mL for PLL, DXS; 1mg/mL for HA, Alg) at pH 7.4 under agitation for 30 min. The particle suspension was purified from the polyelectrolyte solution via centrifugation (15,000 g, 30 min), and this process was repeated iteratively for deposition of each layer. Final particle suspensions were characterized by dynamic light scattering (DLS) and zeta potential analysis (Malvern Instruments, ZS90) and stored at 4°C prior to testing.

in vitro Drug Release

Particle formulations were suspended in 1X PBS and incubated in 2 mL dialysis float-a-lyzers (3.5KDa MWCO) while agitated at 37°C in 1X PBS under sink conditions. Small

aliquots were collected at various time points, replaced with fresh solution, and analyzed by high-performance liquid chromatography (HPLC, Agilent Technologies).

in vivo experimentation

For biodistribution experiments, NCR nude female mice (Taconic) were used. To attenuate gut fluorescence, an alfalfa-free special diet (AIN-93M Maintenance Purified Diet from TestDiet) was administered to the mice 1 week prior to and during experimentation. Nanoparticle formulations suspended in 1X PBS were administered via the tail vein. *In vivo* imaging (IVIS, Caliper Instruments) was performed at regular time points. Full scale biodistribution harvesting of relevant organs was conducted at a relevant time point and imaged using the IVIS to quantify recovered fluorescence. Circulation persistence experiments were performed in BALB/c female mice from Taconic. Nanoparticle formulations were administered via the tail vein. Blood collection was obtained from the retro-orbital sinus (~0.2–0.3mL, diluted in ~0.1mL 0.5 M EDTA) and imaged using the IVIS to quantify recovered fluorescence. For cardiogreen recovery experiments, feces were recovered from three BALB/c mice per experimental group and fractional recovered fluorescence (IVIS) was quantified across a 48 h window. For co-injection experiments, free polymer corresponding to the terminal layer polymer used for the NP architecture being investigated were diluted in PBS and co-injected at normalized concentrations of particles against 10 mg/kg and 20 mg/kg free polymer in NCR mice. Experiments were performed under the guidance and supervision of the MIT Department of Comparative Medicine and Committee on Animal Care.

in vitro opsonization experimentation

Texas Red-labeled polymer nanoparticles (company) were incubated with fluorescently labeled protein (Human IgG-FITC, Sigma) for 1h. Bound protein was quantified using a nanodrop spectrophotometer (GE Nanovue Plus). These particles were subsequently incubated with the murine macrophage cell line (J774A.1, ATCC) for 1h and cell-associated fluorescence was quantified via fluorescence-activated cell sorting (BD LSR II). Geometric mean cell-associated fluorescence was used for display of particle association with the cells.

Results and Discussion

The schematic for generating films using electrostatic LbL assembly is presented in Figure 1A. The PLGA core particles used in this work are generated from carboxylic acid terminated PLGA, and present a net negative charge on their surfaces, which provide a means for initiating LbL assembly. Iterative adsorption of alternately charged polyelectrolytes is accomplished by incubation of particles in aqueous polycation and polyanion solutions, with intermediate rinse steps, to generate LbL nanoparticles. Although this study focuses on the materials tabulated in Supplemental Table 1, a much larger library of film components, along with a diverse range of therapeutics, can be generated for incorporation on this platform. Towards this end, materials with relevant biological functionalities are of particular interest, such as negatively-charged linear polysaccharides including hyaluronic acid (HA), dextran sulfate (DXS), and alginate (Alg). Each of these polysaccharides have demonstrated anti-fouling properties as hydrophilic brush-like

hydrated coatings to minimize protein adsorption and opsonization[36–39]; as such, they present promising biodegradable, biomimetic alternatives to the traditional and widely-reported use of poly(ethylene glycol).[40] Further, HA is a known ligand for CD44 receptors[41], which are characteristically overexpressed in many aggressive cancer cell types, including triple-negative breast cancer.[42] Alg is known to be an essential protective coating for pathogenic bacteria to evade host immune responses.[43] Each of these materials has been incorporated in the current study.

Characterization of the resulting LbL particles is shown with regard to particle hydrodynamic size and charge in Figures 1B and 1C. Following deposition of six layers on a 125 nm diameter polymer core, particles range in hydrodynamic size from 180nm for DXS-terminated NPs to 250nm for Alg-terminated NPs, based on a number distribution. The dynamic light scattering data taken as a function of the number of deposited bilayers indicates that the nanoparticles grow at a rate of approximately 18 nm in diameter with each bilayer pair, corresponding to nanolayer thickness increases of 9 nm per adsorbed polymer pair, over the first five adsorbed layers. This relatively linear growth is consistent with traditional LbL processes.[44] The three different LbL film architectures are similar in size until the sixth and final adsorbed polyanion layer. The DXS-terminated LbL nanoparticles continue to grow linearly; whereas the particles terminated with HA and Alg both indicate a significant increase in thickness with the final adsorbed layer, which is 55 and 77 nm, respectively. In LbL assembly, it has been observed that the thickness and density of the layer deposited is highly dependent on pH for weak polyelectrolytes due to changes in the degree of ionization along the backbone.[45] Furthermore, certain weakly charged polyelectrolytes, including hyaluronic acid, can undergo exponential growth behavior due to interdiffusion of the absorbing species above a critical thickness.[46, 47] This increased increment may be further impacted by the high degree of hydration of the high molecular weight HA (500K MW) and Alg (200K MW) backbones, and to the partially charged nature of the carboxylic acid groups along the glycopolymer backbone. The surface charge of the particles is reversed with each deposition step, confirming that the film is building in a stepwise fashion driven by alternating electrostatic adsorption. The overall surface potential was (+/−) 50–60mV (in ultrapure 18 MΩ water, 25°C), independent of terminal layer.

Previous work established a minimum number of four layers for generation of serum-stable particles, with diminishing returns beyond eight layers.[28] Independent optimization conducted for the current PLGA-based particle template was found to be consistent with these findings; therefore, this study reports data from six-layered (6L) particles with the following nanoparticle architecture: a biodegradable PLGA nanoparticle core (acid-terminal, hydrodynamic diameter = 125nm; ζ-potential = −50mV) containing a drug, which is layered with polycationic/polyanionic pairs deposited iteratively on top of this substrate, terminated with a final polyanion. The systems were assembled with poly-L-lysine (PLL) as the polycation and DXS as the intermediate polyanion, and are indicated as $PLGA_{drug}/(PLL/DXS)_2/PLL/X_{term}$, where X_{term} is either HA, Alg, or DXS.

To facilitate our investigation of the *in vivo* fate of drug cargo after systemic circulation, we sought a good candidate for a conventional chemotherapeutic, doxorubicin (logP (pH 7.4) = 1.27), which inhibits topoisomerase II, resulting in DNA damage thus disabling cellular

replication. The model drug chosen for systematic stability assessments of different nanoparticle architectures is cardiogreen (CG, λ_{ex} = 740nm, λ_{em} = 820nm, logP (pH 7.4) = −0.29), a hydrophilic near-IR dye that absorbs light at 820nm, where there is minimal whole-animal auto-fluorescence. The fundamental chemical characteristics of both small molecules are also similar; they are hydrophilic with low molecular weights (543.5 g/mol for doxorubicin and 775g/mol for CG) and are significantly charged (pI_{CG} = 3.3; pI_{Dox} = 11) under physiological conditions with water solubilities in the range of 1mg/mL and similar lipophilicities ($logP_{CG}$ = −0.29; $logP_{Dox}$ = 1.27; pH 7.4). Additionally, CG is cleared from circulation readily, with a serum half-life of 2–3 minutes (compared to 10 minutes for doxorubicin),[48] and in a manner that traffics exclusively via the liver, such that its clearance from the body can be monitored in the liver and gall bladder via *in vivo* imaging, and corroborated with recovered fluorescence from the feces in addition to the relevant biodistribution and blood sampling.[49] These advantageous properties make CG a particularly good choice to model the *in vivo* fate of small molecule therapeutics in systemic delivery carriers, as multiple readouts, including biodistribution, persistence data via blood and feces collection, are generated from a single animal to guide particle engineering.

To demonstrate the similarity of CG to conventional small molecule chemotherapeutics, release profiles for both doxorubicin and CG were determined for the uncoated NP core as well as the layered LbL nanoparticle architectures under physiological conditions (37°C, stirred in large excess of 1X phosphate buffered saline (PBS)) using high performance liquid chromatography (HPLC) to determine quantitative and fractional release. The resulting release curves for these two molecules are compared in Figures 2A and 2B. The *in vitro* release characteristics are similar, with both exhibiting the same general release profiles and similar fractional release in the coated (60% released after 48h, following from initial drug loadings of 10ug/mL for CG-loaded NP formulations and 50ug/mL for Dox-loaded NP formulations) and uncoated (100% released after 48h) versions, proving CG to be an effective model of doxorubicin for the demonstration of LbL NP technologies as small molecule delivery agents. The observed release kinetics is typical of biodegradable particle cores and consistent with mathematical models accounting for small molecule diffusion-based release (initial logarithmic-phase release) and bulk erosion (inflection after initial diffusion-based release plateaus) of the PLGA matrix.[50–52] The characteristic diffusion-erosion based release is observed for both coated and uncoated systems; however, the LbL coated systems show significant benefit in small molecule sequestration, minimizing the characteristic bolus release observed initially (from ~35% uncoated core to ~20% coated after 1h), and sustaining release of the therapeutic over longer time scales of up to 4–5 days *in vitro*. Greater control and modulation of bolus release is important to diminish systemic toxicity while the nanoparticle is en route to the tumor site, particularly for cytotoxic chemotherapeutics. Extended release of drug from the nanoparticle once it has reached its target location may also have therapeutic value for certain types of molecular drugs. The variable terminal layer had little to no effect on overall release profiles, despite the range of functionalities and molecular weights used for the end-capping layer. Drug release from the NP is characteristic of the bulk film properties of the LbL multilayer, and relatively independent of the end-capping layer. It thus appears that the terminal layer primarily serves as a functional interface directing the biodistribution and blood circulation behavior of the

delivery system, while the bulk film impacts the pharmacokinetics of the encapsulated therapeutic. These findings suggest the LbL nanoparticle technology can provide a modular platform for systemic drug delivery.

To understand the impact of these particle architectures on the pharmacokinetics of the model drug and nanocarrier used for delivery, simultaneous tracking of both the near-IR labeled polycationic layer 1, PLL_{700} (modified with Cy5.5 dye, $\lambda_{ex,max}$ = 673 nm, $\lambda_{em,max}$ = 707 nm), and encapsulated model drug, CG, was conducted using *in vivo* imaging (IVIS) following systemic administration via the tail vein. This approach to systematically screen libraries of LbL NP architectures as therapeutic vehicles is an exciting, novel means of generating multiple readouts, including biodistribution and persistence in the animal (blood, feces sampling), from longitudinal studies of animals. In this way, nanoparticle stability and its pharmacokinetic behavior is assessed based on persistence in circulation and biodistribution over time at λ_{ex} = 640 nm, λ_{em} = 700 nm (PLL_{700} channel), while drug stability and pharmacokinetics is also evaluated by biodistribution and circulation data, as well as recovered drug fluorescence in feces as a function of time at λ_{ex} = 745 nm, λ_{em} = 820 nm (CG_{820} channel). Due to the hepatic-specific clearance of CG, the feces serve as a quantitative measure of drug clearance from the animal to further assess drug bioavailability as a function of time with each NP system investigated.

The IVIS images achieved for biodistribution studies are shown in Figure 3 for both the drug (3A) and NP (3B) channel. Significant differences in the accumulated signal intensities were observed for different formulations of the layered architectures in the liver, relative to the controls, within the first 30 minutes post-administration on both the PLL_{700} and CG_{820} channels. Normalization of the liver-associated CG fluorescence (circled and identified with an arrow) with total fluorescence from the amount injected, shows significant reduction of CG accumulation in the liver when administered as cargo in LbL-NPs versus free or uncoated PLGA NPs. The quantified signal for liver accumulation at 5 minutes post-injection for the free drug (70%) and uncoated nanoparticle (55%) formulations are much higher when compared to the layered architectures, Alg-term (15%), HA-term (17%), and DXS-term (28%). At the carrier channel for PLL_{700}, 50% injected dose is associated with the liver after 5 minutes for free PLL_{700}, as compared to 12% for Alg-terminated 6L NPs, 15% for HA500K-terminated, 25% for DXS-terminated. The full 48h stability panels at both channels are shown in Supplemental Figures 1 and 2, with quantification of the total radiant efficiency from the whole animal as a function of time displayed for the panel of images at each channel to gauge persistence of the individual NP components (drug, particle). These data reflect the improved biodistribution and overall enhanced persistence of the coated CG-loaded NP formulations, relative to the uncoated polymer-encapsulated and free drug formulations.

The results from *in vivo* whole-animal imaging were further substantiated by harvesting of the relevant clearance organs. This biodistribution data was collected 30 minutes post-administration (Figures 4A and 4B, Supplemental Figure 3). Significantly reduced drug clearance is evident for the coated systems within the first 30 minutes post-injection, with 55% ID/g associated with the liver after 30 minutes for free cardiogreen, as compared to 43% for the uncoated PLGA CG-loaded core, 33% for DXS-terminated, 18% for HA-

terminated, and 20% Alg-terminated systems. Layered architectures also exhibit minimal clearance during this time frame as delivery carriers, with 70% ID/g associated with the liver for control free PLL_{700}, 32% for DXS-terminated, 20% for Alg-terminated systems, and 22% for HA-terminated systems. The similarity in percent recovery of fluorescence between the particle and drug channel from this biodistribution data, along with the *in vivo* images in Figure 3, illustrate co-localization of the drug with the delivery platform for the initial period post-administration (up to 4h); however, as shown in Supplemental Figures 1 and 2, this does not hold at long time points. At 8h and beyond, due to small molecule out-diffusion ("leakage") from the LbL NP and subsequent bulk-erosion based release observed *in vitro*, the particle and drug localize in the liver at different times.

Further, recovered fluorescence from the feces can also serve as readouts for drug clearance in the animal. As shown in Figure 4C, CG is recovered in the bile following longer time intervals for the coated systems. The DXS-terminated system peaks in fractional CG recovery at only the 4–8h time span post-injection as compared to Alg- and HA-terminated systems, which peak in the 8–12h time period. This further corroborates the enhanced persistence and drug bioavailability that the coated delivery systems can promote.

To try to rationalize the observed differences in feces drug recovery and biodistribution of DXS-terminated systems as compared to the other two coated systems, we hypothesized that, as previously implicated,[53, 54] the sulfonated polysaccharide dextran sulfate preferentially binds liver receptors (e.g. liver endothelial cells, Kupffer cells) that scavenge blood for soluble macromolecules. From the biodistribution and feces recovery results, it is clear that HA- and Alg-terminated systems delay particle and drug clearance as well as exhibit improved biodistribution. These results implicate that this potential receptor-mediated mechanism for clearance impacts drug biodistribution as well as that for the carrier agent. This is further illustrated by co-injection of free terminal layer polymer with the corresponding polymer-terminated 6-layered NP. Significant reduction in CG signal was observed only when free DXS was co-injected with the DXS/sulfonate-terminated NPs, as evident in Figure 4D. Free polymer competition for receptor-binding suggests that the sulfonated terminal layer preferentially interacts with the liver endothelial cells,[54, 55] promoting receptor-mediated endocytosis that significantly affects the clearance of DXS-terminated LbL particles. The differential impact of a co-injection of free terminal layer polymer was quantified by normalizing the liver-associated fluorescence obtained from co-injection studies with signal intensities for particle-only studies (30 minute stability panel shown in Supplemental Figure 4). No effect was observed for corresponding co-injections with Alg- and HA-terminated systems, in contrast to DXS-terminated nanoparticles, with liver-associated uptake, implying receptor-independent liver uptake.

Additionally, *in vitro* opsonization of the different NP architectures (Supplemental Figure 7) showed little dependence on protein adsorption and no dependence on subsequent macrophage-associated fluorescence as a function of terminal layer choice, further suggesting that all coatings have similar protein resistive properties and that the mononuclear phagocyte system clearance is likely not the primary reason for the different liver signal intensities (respective to uncoated and PLL controls). Poorer biodistribution of the DXS-terminated particles results relative to other coatings guided particle and drug

persistence experiments for only the more optimal systems, HA- and Alg-terminated particles. Results on drug and carrier stability in circulation for these systems are presented in Figures 4E and 4F (raw data shown in Supplemental Figure 5). The particles exhibit improved pharmacokinetic properties in circulation, with Alg-terminated NPs characterized by half-lives, based on a two-compartment model, of 0.59h and 7.18h and HA-terminated NPs characterized by half-lives of 0.50h and 7.861h. The lifetime of drug from these platforms is also, compared to the reported free drug half-life of 2 min and uncoated $PLGA_{CG}$ core half-lives of 0.15h and 1.87h, extended to 0.52h and 4.17h for Alg-terminated NPs and, for HA-terminated NPs, to 0.48h and 4.54h (based on a 2-compartment model).

These findings are consistent with previously reported PEGylated versions of PLGA nanoparticles that show 30–65% particles remaining (for various MW PEG shells) in serum 3h post-i.v. administration with liver-associated clearance of the particles remaining at or below 20% up to 5h post-administration.[56] This is important because, in addition to imparting similar hydration properties to the particle surface like PEG, LbL can also provide a surface that is molecularly targeted for cellular engagement and/or cue-sensitive (e.g. pH-responsive[30]) for exploiting the cellular environment in hypoxic tumor compartments. Alternatively, PEG can be used exclusively as a hydration layer for minimizing protein adsorption, opsonization, and subsequent clearance by the major players in the mononuclear phagocyte system (MPS) system – a property that in fact can also negatively impact interactions with target cells.[57, 58] These findings clearly highlight the benefit of LbL-functionalized nanoparticle systems as extended release platforms, particularly for small molecule therapeutics, allowing for enhanced drug and particle persistence in circulation and that promote hydrated, protein-resistive properties for more efficacious systemic drug delivery. This provides much promise towards development of these systems as molecularly targeted entities, in addition to improved biological performance observed in this investigation.

Small molecule sequestration in delivery platforms for extended periods in circulation remains a significant challenge to selective delivery of therapeutics to the target tissue;[32] however, the coatings investigated here demonstrate an enhanced level of control over diffusional bolus release following administration, as well as an ability to enhance the circulation half-life for longer periods of time *in vivo.* The findings in this investigation, namely the improved pharmacokinetic behavior observed with Alg- and HA-terminated NPs via biodistribution, feces drug recovery, and persistence in circulation, are consistent with documented anti-fouling characteristics of HA[59–61] and Alg.[39, 53, 62] These systems present exciting new opportunities for enhancing delivery of small molecule therapeutics; however, due to the accelerated rate at which the uncoated PLGA drug-loaded core is hydrolytically degraded and unloaded in circulation (with short half-lives and poor biodistribution, see Supplementary Figure 6), the LbL system can be further adapted to different core materials and encapsulation approaches (e.g. covalent attachment of therapeutics to core materials or film components), which is currently under active investigation in our laboratory to probe whether the benefits of enhanced persistence, improved biodistribution, and controlled drug release provided by LbL-coated systems will promote more efficacious EPR-based and molecular targeting strategies.

Conclusion

LbL is a facile approach for generating functional thin films for enhanced systemic delivery of nanoscopic systems. This self-assembly method allows for incorporation of a broad range of materials; and due to its water-based synthesis, it allows for incorporation of a diverse set of therapeutics without significant alteration of biological function. To facilitate continued development of these systems, the current study establishes a two color imaging methodology that enables efficient, high throughput *in vivo* screening of a library of material architectures and establishes each as systemic drug carriers. Using live animal *in vivo* imaging, multiple readouts, including biodistribution, persistence, and feces drug recovery can be performed, longitudinally assessing *in vivo* fate of both particle and drug in a single animal model. Further, this work demonstrates LbL-drug delivery particles with enhanced persistence and improved drug/carrier biodistribution using biomimetic alternatives to poly(ethylene glycol), specifically Alg and HA, as terminal layers for this NP delivery vehicle. In total, LbL provides a powerful tool to engineer NP systems that control drug release while incorporating materials that are dynamic, protein-resistive, and molecularly-targeted for more efficacious systemic treatment of diseased states.

Supplementary Material

Refer to Web version on PubMed Central for supplementary material.

Acknowledgments

We would like to thank funding from Janssen Pharmaceuticals TRANSCEND for supporting this work. We would also like to thank the Koch Institute for Integrative Cancer Research at MIT for providing facilities to support this work, as well as DCM (Department of Comparative Medicine, MIT) for assistance with animal experiments and facilities. S.W.M. would also like to acknowledge a National Science Foundation Graduate Research Fellowship (NSF GRF).

References

1. Decher G. Fuzzy nanoassemblies: toward layered polymeric multicomposites. Science. 1997; 277:1232–7.
2. Panyam J, Labhasetwar V. Biodegradable nanoparticles for drug and gene delivery to cells and tissue. Adv Drug Deliv Rev. 2003; 55:329–47. [PubMed: 12628320]
3. LaVan DA, Lynn DM, Langer R. Moving smaller in drug discovery and delivery. Nat Rev Drug Discov. 2002; 1:77–84. [PubMed: 12119612]
4. Hammond PT. Building biomedical materials layer-by-layer. Mater Today. 2012; 15:196–206.
5. Hammond PT. Polyelectrolyte multilayered nanoparticles: using nanolayers for controlled and targeted systemic release. Nanomedicine. 2012; 7:619–22. [PubMed: 22630144]
6. Tang Z, Wang Y, Podsiadlo P, Kotov NA. Biomedical applications of layer-by-layer assembly: from biomimetics to tissue engineering. Adv Mater. 2006; 18:3203–24.
7. Chen F-M, Zhang M, Wu Z-F. Toward delivery of multiple growth factors in tissue engineering. Biomaterials. 2010; 31:6279–308. [PubMed: 20493521]
8. Cortez C, Tomaskovic-Crook E, Johnston AP, Scott AM, Nice EC, Heath JK, Caruso F. Influence of size, surface, cell line, and kinetic properties on the specific binding of A33 antigen-targeted multilayered particles and capsules to colorectal cancer cells. ACS Nano. 2007; 1:93–102. [PubMed: 19206525]

9. Kamphuis MM, Johnston AP, Such GK, Dam HH, Evans RA, Scott AM, Nice EC, Heath JK, Caruso F. Targeting of cancer cells using click-functionalized polymer capsules. J Am Chem Soc. 2010; 132:15881–3. [PubMed: 20977221]
10. Schneider A, Vodouhe C, Richert L, Francius G, Le Guen E, Schaaf P, Voegel JC, Frisch B, Picart C. Multifunctional polyelectrolyte multilayer films: combining mechanical resistance, biodegradability, and bioactivity. Biomacromolecules. 2007; 8:139–45. [PubMed: 17206799]
11. Facca S, Cortez C, Mendoza-Palomares C, Messadeq N, Dierich A, Johnston AP, Mainard D, Voegel JC, Caruso F, Benkirane-Jessel N. Active multilayered capsules for in vivo bone formation. Proc Natl Acad Sci U S A. 2010; 107:3406–11. [PubMed: 20160118]
12. De Geest BG, De Koker S, Sukhorukov GB, Kreft O, Parak WJ, Skirtach AG, Demeester J, DeSmedt SC, Hennick WE. Polyelectrolyte microcapsules for biomedical applications. Soft Matter. 2009; 5:282–91.
13. Caruso F. Nanoengineering of particle surfaces. Adv Mater. 2001; 13:11–22.
14. Becker AL, Johnston APR, Caruso F. Layer-by-layer-assembled capsules and films for therapeutic delivery. Small. 2010; 6:1836–52. [PubMed: 20715072]
15. Reibetanz U, Claus C, Typlt E, Hofmann J, Donath E. Defoliation and plasmid delivery with layer-by-layer coated colloids. Macromol Biosci. 2006; 6:153–60. [PubMed: 16456874]
16. Gittins DI, Caruso F. Tailoring the polyelectrolyte coating of metal nanoparticles. J Phys Chem B. 2001; 105:6846–52.
17. Gittins DI, Caruso F. Multilayered polymer nanocapsules derived from gold nanoparticle templates. Adv Mater. 2000; 12:1947–9.
18. Mayya KS, Schoeler B, Caruso F. Preparation and organization of nanoscale polyelectrolyte-coated gold nanoparticles. Adv Funct Mater. 2003; 13:183–8.
19. Elbakry A, Zaky A, Liebl R, Rachel R, Goepferich A, Breunig M. Layer-by-layer assembled gold nanoparticles for siRNA delivery. Nano Lett. 2009; 9:2059–64. [PubMed: 19331425]
20. Lvov YM, Pattekari P, Zhang X, Torchilin V. Converting poorly soluble materials into stable aqueous nanocolloids. Langmuir. 2010; 27:1212–7. [PubMed: 21190345]
21. Schneider GF, Subr V, Ulbrich K, Decher G. Multifunctional cytotoxic stealth nanoparticles: a model approach with potential for cancer therapy. Nano Lett. 2009; 9:636–42. [PubMed: 19170551]
22. Pattekari P, Zheng Z, Zhang X, Levchenko T, Torchilin V, Lvov Y. Top-down and bottom-up approaches in production of aqueous nanocolloids of low solubility drug paclitaxel. Phys Chem Chem Phys. 2011; 13:9014–9. [PubMed: 21442095]
23. Shutava TG, Balkundi SS, Vangala P, Steffan JJ, Bigelow RL, Cardelli JA, O'Neal DP, Lvov Y. Layer-by-layer-coated gelatin nanoparticles as a vehicle for delivery of natural polyphenols. ACS Nano. 2009; 3:1877–85. [PubMed: 19534472]
24. Yuk SH, Oh KS, Cho SH, Kim SY, Oh S, Lee JH, Kim K, Kwon IC. Enhancement of the targeting capabilities of the paclitaxel-loaded pluronic nanoparticles with a glycol chitosan/heparin composite. Mol Pharm. 2012; 9:230–6. [PubMed: 22149139]
25. Zhao Q, Han B, Wang Z, Gao C, Peng C, Shen J. Hollow chitosan-alginate multilayer microcapsules as drug delivery vehicle: doxorubicin loading and in vitro and in vivo studies. Nanomedicine. 2007; 3:63–74. [PubMed: 17379170]
26. Sexton A, Whitney PG, Chong S-F, Zelikin AN, Johnston APR, De Rose R, Brooks AG, Caruso F. A protective vaccine delivery system for in vivo t cell stimulation using nanoengineered polymer hydrogel capsules. ACS Nano. 2009; 3:3391–400. [PubMed: 19824668]
27. Zheng Z, Zhang X, Carbo D, Clark C, Nathan C, Lvov Y. Sonication-assisted synthesis of polyelectrolyte-coated curcumin nanoparticles. Langmuir. 2010; 26:7679–81. [PubMed: 20459072]
28. Poon Z, Lee JB, Morton SW, Hammond PT. Controlling in vivo stability and biodistribution in electrostatically assembled nanoparticles for systemic delivery. Nano Lett. 2011; 11:2096–103. [PubMed: 21524115]
29. Maeda H, Nakamura H, Fang J. The EPR effect for macromolecular drug delivery to solid tumors: Improvement of tumor uptake, lowering of systemic toxicity, and distinct tumor imaging in vivo. Adv Drug Deliv Rev.

30. Poon Z, Chang D, Zhao X, Hammond PT. Layer-by-layer nanoparticles with a pH-sheddable layer for in vivo targeting of tumor hypoxia. ACS Nano. 2011; 5:4284–92. [PubMed: 21513353]
31. Yang X-Z, Du J-Z, Dou S, Mao C-Q, Long H-Y, Wang J. Sheddable Ternary Nanoparticles for tumor acidity-targeted siRNA delivery. ACS Nano. 2011; 6:771–81. [PubMed: 22136582]
32. Chen Z. Small-molecule delivery by nanoparticles for anticancer therapy. Trends Mol Med. 2010; 16:594–602. [PubMed: 20846905]
33. Shukla A, Fuller RC, Hammond PT. Design of multi-drug release coatings targeting infection and inflammation. J Control Release. 2011; 155:159–66. [PubMed: 21699932]
34. Smith RC, Riollano M, Leung A, Hammond PT. Layer-by-layer platform technology for small-molecule delivery. Angew Chem Int Ed Engl. 2009; 48:8974–7. [PubMed: 19847838]
35. Kwon H-Y, Lee J-Y, Choi S-W, Jang Y, Kim J-H. Preparation of PLGA nanoparticles containing estrogen by emulsification–diffusion method. Colloids Surf A Physicochem Eng Asp. 2001; 182:123–30.
36. Perrino C, Lee S, Choi SW, Maruyama A, Spencer ND. A biomimetic alternative to poly(ethylene glycol) as an antifouling coating: resistance to nonspecific protein adsorption of poly(L-lysine)-graft-dextran. Langmuir. 2008; 24:8850–6. [PubMed: 18616303]
37. Lee Y, Lee H, Kim YB, Kim J, Hyeon T, Park H, Messersmith PB, Park TG. Bioinspired surface immobilization of hyaluronic acid on monodisperse magnetite nanocrystals for targeted cancer imaging. Adv Mater. 2008; 20:4154–7. [PubMed: 19606262]
38. Morra M, Cassineli C. Non-fouling properties of polysaccharide-coated surfaces. J Biomater Sci Polym Ed. 1999; 10:1107–24. [PubMed: 10591135]
39. Kodiyan A, Silva EA, Kim J, Aizenberg M, Mooney DJ. Surface modification with alginate-derived polymers for stable, protein-repellent, long-circulating gold nanoparticles. ACS Nano. 2012; 6:4796–805. [PubMed: 22650310]
40. Knop K, Hoogenboom R, Fischer D, Schubert US. Poly(ethylene glycol) in drug delivery: pros and cons as well as potential alternatives. Angew Chem Int Ed Engl. 2010; 49:6288–308. [PubMed: 20648499]
41. Culty M, Shizari M, Thompson EW, Underhill CB. Binding and degradation of hyaluronan by human breast cancer cell lines expressing different forms of CD44: correlation with invasive potential. J Cell Physiol. 1994; 160:275–86. [PubMed: 7518822]
42. Foulkes WD, Smith IE, Reis-Filho JS. Triple-negative breast cancer. N Engl J Med. 2010; 363:1938–48. [PubMed: 21067385]
43. Leid JG, Willson CJ, Shirtliff ME, Hassett DJ, Parsek MR, Jeffers AK. The exopolysaccharide alginate protects pseudomonas aeruginosa biofilm bacteria from IFN-γ-mediated macrophage killing. J Immun. 2005; 175:7512–8. [PubMed: 16301659]
44. Hammond PT. Form and function in multilayer assembly: new applications at the nanoscale. Adv Mater. 2004; 16:1271–93.
45. Shiratori SS, Rubner MF. pH-Dependent thickness behavior of sequentially adsorbed layers of weak polyelectrolytes. Macromolecules. 2000; 33:4213–9.
46. Picart C, Lavalle P, Hubert P, Cuisinier FJG, Decher G, Schaaf P, Voegel JC. Buildup mechanism for poly(L-lysine)/hyaluronic acid films onto a solid surface. Langmuir. 2001; 17:7414–24.
47. Picart C, Mutterer J, Richert L, Luo Y, Prestwich GD, Schaaf P, Voegel JC, Lavalle P. Molecular basis for the explanation of the exponential growth of polyelectrolyte multilayers. Proc Natl Acad Sci U S A. 2002; 99:12531–5. [PubMed: 12237412]
48. Rahman A, Carmichael D, Harris M, Roh JK. Comparative pharmacokinetics of free doxorubicin and doxorubicin entrapped in cardiolipin liposomes. Cancer Res. 1986; 46:2295–9. [PubMed: 3697976]
49. Uusaro A, Ruokonen E, Takala J. Estimation of splanchnic blood flow by the fick principle in man and problems in the use of indocyanine green. Cardiovasc Res. 1995; 30:106–12. [PubMed: 7553712]
50. Faisant N, Siepmann J, Benoit JP. PLGA-based microparticles: elucidation of mechanisms and a new, simple mathematical model quantifying drug release. Eur J Pharm Sci. 2002; 15:355–66. [PubMed: 11988397]

51. Siepmann J, Göpferich A. Mathematical modeling of bioerodible, polymeric drug delivery systems. Adv Drug Deliv Rev. 2001; 48:229–47. [PubMed: 11369084]
52. Heller, J.; Baker, RW. Controlled release of bioactive materials. 1980. New York: Academic Press; 1980. p. 1-18.
53. Gustafson S. The influence of sulfated polysaccharides on the circulating levels of hyaluronan. Glycobiol. 1997; 7:1209–14.
54. Gustafson S, Bjorkman T. Circulating hyaluronan, chondroitin sulphate and dextran sulphate bind to a liver receptor that does not recognize heparin. Glycoconj J. 1997; 14:561–8. [PubMed: 9298688]
55. Alston-Smith JP, Pertoft H, Laurent TC. Endocytosis of hyaluronan in rat kupffer cells. Biochem J. 1992; 286:519–26. [PubMed: 1530585]
56. Avgoustakis K, Beletsi A, Panagi Z, Klepetsanis P, Livaniou E, Evangelatos G, Ithakissios DS. Effect of copolymer composition on the physicochemical characteristics, in vitro stability, and biodistribution of PLGA–mPEG nanoparticles. Int J Pharm. 2003; 259:115–27. [PubMed: 12787641]
57. Owens DE III, Peppas NA. Opsonization, biodistribution, and pharmacokinetics of polymeric nanoparticles. Int J Pharm. 2006; 307:93–102. [PubMed: 16303268]
58. Huynh NT, Roger E, Lautram N, Benoît J-P, Passirani C. The rise and rise of stealth nanocarriers for cancer therapy: passive versus active targeting. Nanomedicine. 2010; 5:1415–33. [PubMed: 21128723]
59. Joester D, Klein E, Geiger B, Addadi L. Temperature-sensitive micrometer-thick layers of hyaluronan grafted on microspheres. J Am Chem Soc. 2006; 128:1119–24. [PubMed: 16433527]
60. Morra M. Engineering of biomaterials surfaces by hyaluronan. Biomacromolecules. 2005; 6:1205–23. [PubMed: 15877335]
61. Thierry B, Winnik FM, Merhi Y, Griesser HJ, Tabrizian M. Biomimetic hemocompatible coatings through immobilization of hyaluronan derivatives on metal surfaces. Langmuir. 2008; 24:11834–41. [PubMed: 18759386]
62. Zhou J, Romero G, Rojas E, Ma L, Moya S, Gao C. Layer by layer chitosan/alginate coatings on poly(lactide-co-glycolide) nanoparticles for antifouling protection and folic acid binding to achieve selective cell targeting. J Colloid Interface Sci. 2010; 345:241–7. [PubMed: 20227712]

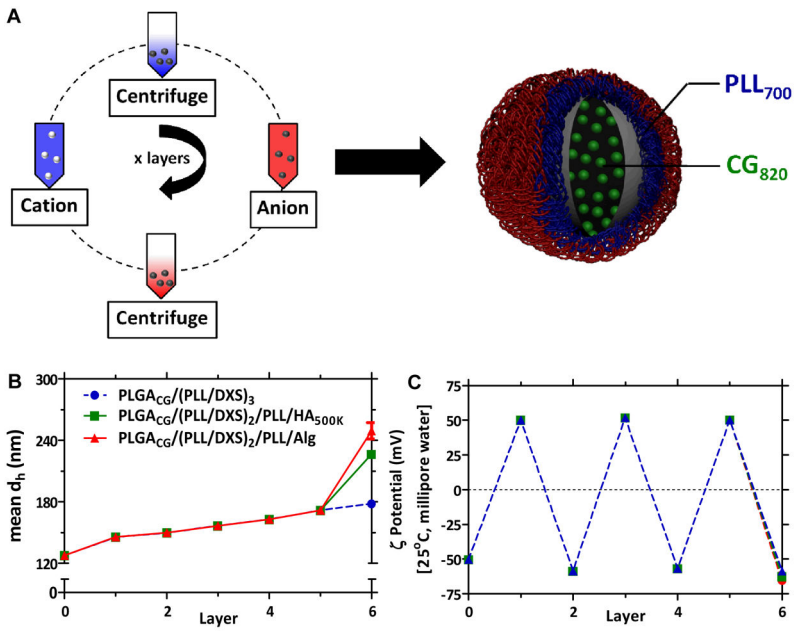

Figure 1. Layer-by-Layer nanoparticle (LbL NP) synthesis and characterization

(A) LbL deposition on NP template. **(B)** Materials library used in current study. **(C)** Representative mean hydrodynamic diameter (based on a number distribution) and **(D)** zeta potential analysis, conducted in ultrapure water at 25°C. All particles in current study are 6 layers (6L) with the following NP architecture: $PLGA^{50:50}_{drug}/(PLL/DXS)_2/PLL/X_{term}$, with drug = doxorubicin (Dox) or cardiogreen (CG) and X_{term} = terminal layer (DXS, Alg, HA_{500K}). (PLGA) poly(lactic-co-clycolic acid), (PLL) poly(L-lysine), (DXS) dextran sulfate, (Alg) alginate, (HA) hyaluronic acid; n = 3, mean +/− SEM. PDI of uncoated PLGA NPs is 0.1; functionalized NPs ranged from 0.15 for DXS-terminated NPs to 0.2–0.25 for HA-coated and Alg-coated NPs. Representative scanning electron micrograph of LbL NPs (HA-coated) shown in Supplemental Image 1.

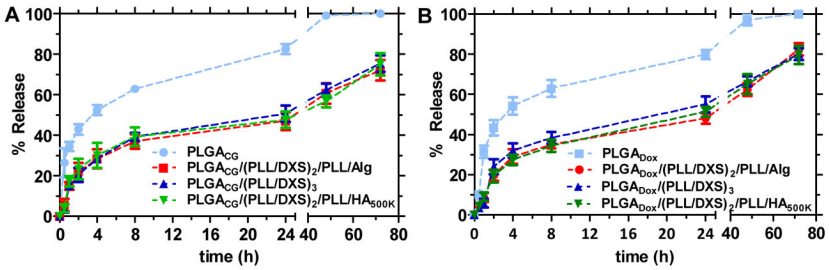

Figure 2. ***In vitro*** **release kinetics of uncoated and coated cargo-loaded cores**

(A) Cardiogreen (CG)-loaded NP formulations and **(B)** Doxorubicin (Dox)-loaded NP formulations in PBS, pH 7.4 at 37C under agitation (3.5KDa MWCO) as measured by high-performance liquid chromatography (HPLC). (PLGA) poly(lactic-co-clycolic acid), (PLL) poly(L-lysine), (DXS) dextran sulfate, (Alg) alginate, (HA) hyaluronic acid, (CG) cardiogreen, (Dox) doxorubicin; n = 3, mean +/− SEM.

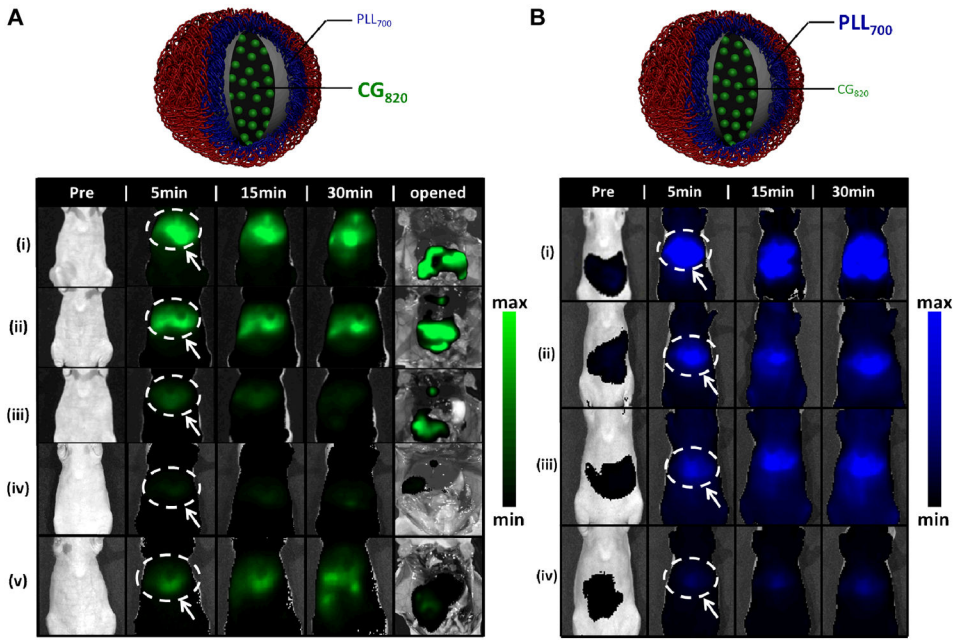

Figure 3. Stability assessments of different nanoparticle architectures using drug (CG_{820}) and particle (PLL_{700}) tracking via *in vivo* imaging. (top of each image panel)

Schematic detailing the fluorescent trackers used for stability assessment of NP architectures. CG_{820} is the cargo encapsulated in the LbL NP architecture with the first polycationic layer of the 3 bilayer structure labeled with Cy5.5. **(A) CG_{820} stability panel, surveying drug bioavailability up to 30 minutes post-injection. (i)** free CG_{820}; **(ii)** $PLGA^{50:50}{}_{CG}$; **(iii)** HA-terminated 6L NP; **(iv)** Alg-terminated 6L NP; **(v)** DXS-terminated 6L NP. Representative 48 h study shown in Supplemental Figure 1. IVIS images at CG channel (λ_{ex} = 745 nm, λ_{em} = 820nm), surveyed up to 30 min and subsequently opened. Region of interest analysis shows ~70% injected dose associated with the liver (white dashed circle identified with an arrow) after 5 minutes for free CG, ~55% for $PLGA^{50:50}{}_{CG}$, ~28% for DXS-terminated and ~15% for Alg- and HA_{500K}-terminated 6L NPs; n = 3. **(B) Carrier stability panel, surveying nanoparticle biodistribution up to 30 minutes post-injection. (i)** free PLL_{700}; **(ii)** DXS-terminated 6L NP; **(iii)** HA-terminated 6L NP; **(iv)** Alg-terminated 6L NP. Nanoparticle tracking facilitated by labeling of first polycationic layer (PLL) in 6L NP architecture with Cy5.5. Representative 48 h study shown in Supplemental Figure 2. IVIS images at PLL_{700} carrier channel (λ_{ex} = 640 nm, λ_{em} = 700 nm) were surveyed up to 30 minutes. Region of interest analysis yields ~50% injected dose associated with the liver (white dashed circle identified with an arrow) after 5 minutes for free PLL_{700}, as compared to ~25% for DXS-terminated, ~15% for HA500K-terminated, ~12% for Alg-terminated 6L NPs. (PLGA) poly(lactic-co-clycolic acid), (PLL) poly(L-lysine), (DXS) dextran sulfate, (Alg) alginate, (HA) hyaluronic acid, (CG) cardiogreen; n = 3.

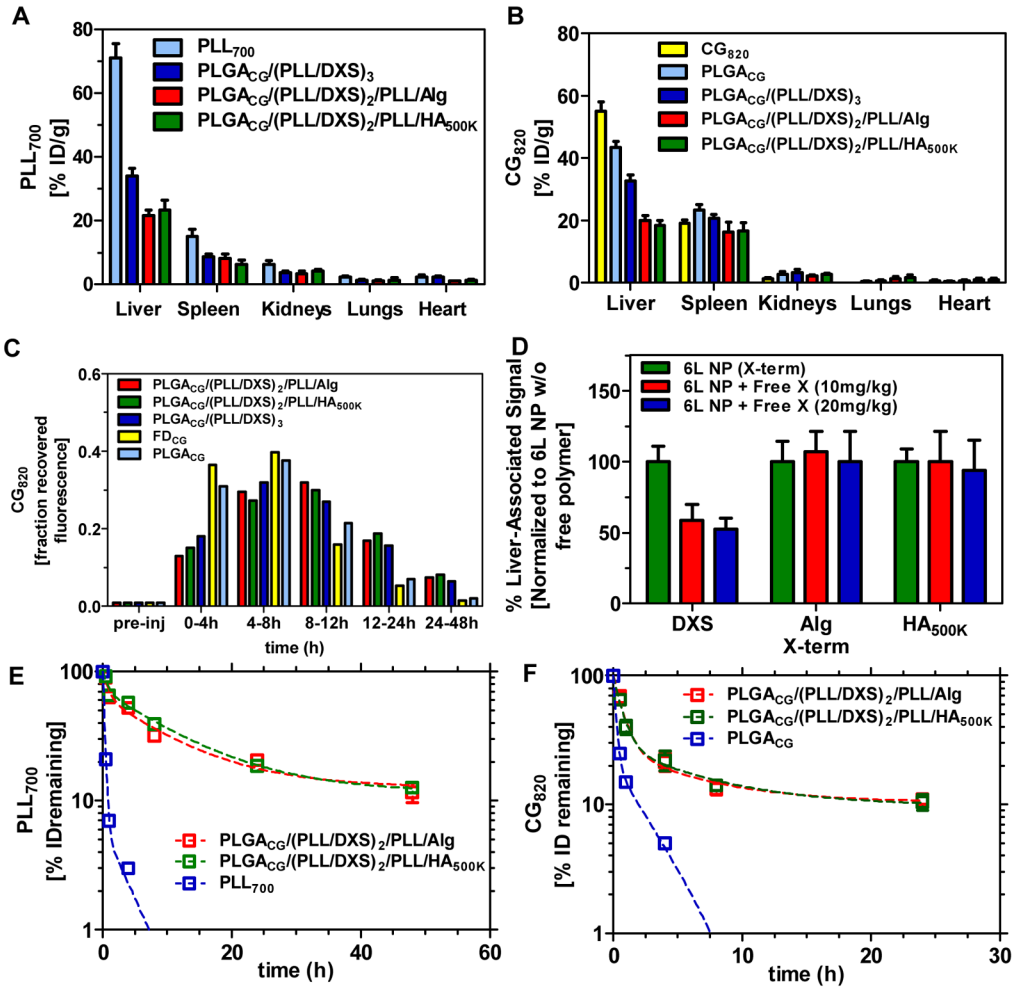

Figure 4. Pharmacokinetic data for the nanocarriers (PLL_{700}, CG_{820}), as a function of terminal layer and the encapsulated drug, CG_{820}

(A, B) Biodistribution profile of carrier via PLL_{700} tracking (λ_{ex} = 640nm, λ_{em} = 700 nm and CG_{820} (λ_{ex} = 745 nm, λ_{em} = 820 nm) 30 minutes post-injection (n=3). Raw data shown in Supplemental Figure 3. (C) Profile of CG recovery in murine feces (3 total mice feces/ experimental group). λ_{ex} = 745 nm, λ_{em} = 820 nm. Data presented as fraction initial dose over a 48h period. **(D)** Dose-dependent co-injection of free polymer with corresponding polymer-terminated 6L NP. Liver-associated CG_{820} fluorescence (λ_{ex} = 745 nm, λ_{em} = 820 nm) collected 15 min following iv administration. Data normalized to average value associated with 6L NP without free polymer co-injection. Raw data shown in Supplemental Figure 4. (E, F) Circulation profile of CG_{820}-loaded NP formulations for both the carrier (λ_{ex} = 640 nm, λ_{em} = 700 nm and encapsulated drug (CG_{820}). Raw data shown in Supplemental Figure 5. (PLGA) poly(lactic-co-clycolic acid), (PLL) poly(L-lysine), (DXS) dextran sulfate, (Alg) alginate, (HA) hyaluronic acid, (CG) cardiogreen; n = 3, mean +/− SEM.